




Comparison of Pulsed Electroacoustic Measurements and AF-NUMIT3 Modeling of Polymers Irradiated with Monoenergetic Electrons

Zachary Gibson* and J. R. Dennison[†] 
Utah State University, Logan, Utah 84322

Brian Beecken[‡]
Bethel University, St. Paul, Minnesota 55101

and
Ryan Hoffmann[§]
Air Force Research Laboratory, Albuquerque, New Mexico 87117

<https://doi.org/10.2514/1.A35519>

Successful spacecraft design and charging mitigation techniques require precise and accurate knowledge of charge deposition profiles. This paper compares models of charge deposition and transport using a venerable deep dielectric charging code, AF-NUMIT3, with direct measurements of charge profiles via pulsed electroacoustic (PEA) measurements. Eight different simulations were performed for comparison to PEA experiments of samples irradiated by 50 or 80 keV monoenergetic electrons in vacuum and at room temperature. Two materials, polyether-ether ketone (PEEK) and polytetrafluoroethylene (PTFE), were chosen for their very low conductivities so that minimal charge migration would occur between irradiation and PEA measurements. PEEK was found to have low acoustic attenuation, while PTFE has high acoustic attenuation through the sample thicknesses of 125 and 250 μm for each material. The measurements were directly compared to AF-NUMIT3 simulations to validate aspects of the code and to investigate the importance of various simulation options, as well as to characterize the PEA instrumentation, measurement methods, and signal processing used. The measurement and simulation values for magnitude of charge deposition, penetration depth, and charge deposition spatial profiles are largely in agreement, though spatial and temporal distributions in incident electron flux and effects of radiation-induced conductivity (RIC) and delayed RIC during the deposition process complicate the process. This work provides an experimental validation of the AF-NUMIT3 deep dielectric charging code and insight into the accuracy and precision of the PEA method.

I. Introduction

KNOWLEDGE of the spatial distribution and temporal evolution of embedded charge in dielectric materials is important in a variety of applications, including semiconductor devices, high-power electronic devices, high-voltage DC cabling, high-energy physics facilities, plasma chambers, and spacecraft charging [1,2]. Electrostatic discharge events are the leading cause of spacecraft failure due to the space environment and cause the majority of space-environment-induced anomalies [3–6]. As satellites orbit, they gain excess charge by interacting with plasma, solar wind, and trapped charges in the space environment. To mitigate charging, accumulation and transport of embedded charge must be understood and predicted. This can be accomplished either by recreating a space environment in the laboratory and measuring the resulting charge distributions or by simulation with models.

Charging codes can simulate charging of materials much more quickly and easily than through experimentation. Simulation also allows for scenarios that may not be feasible through experimentation, thereby facilitating exploration of a broader range of param-

eters. However, it is of great importance to validate these codes experimentally to have the highest confidence in the results and an understanding of their limitations.

There are several charging models in use, including *MCICT* [7,8], *DICTAT* [9,10], *THEMIS* [7], *GEANT4* [11], *GEANT4-RIC* [12], and *NUMIT* [13–16]. There has been a divergence of the *NUMIT* code since its original inception by the late A. R. Frederickson [17,18]. One version has been adapted by Jet Propulsion Laboratory (JPL) as *NUMIT 2.1* [15], as well as a 3D version *NUMIT 3D* [16]. This paper will focus on experimental validation of *AF-NUMIT3*, an adaptation of *NUMIT* developed at the Air Force Research Laboratory (AFRL) by Brian Beecken [13,19,20].

The key parameter in dielectric breakdown is the electric field. Internal electric fields can either be approximated indirectly through measurements such as probing surface potential [21] or determined directly by measurements of the internal charge distribution via methods such as the pulsed electroacoustic (PEA) method [1,27]. The PEA method is a well-established method for nondestructive measurements of embedded charge distributions in dielectric materials. There has been much work done to experimentally validate charging models [7,10,27–29]. Most relevant to this study was an attempt to directly measure internal potentials of electron irradiated materials by layering materials and electrodes and comparing to JPL's *NUMIT 2.0* [30].

However, to the knowledge of the authors there are no published attempts to validate any version of *NUMIT* with direct measurements of the charge distribution via the PEA method, aside from one recent study by some of the authors [19]. PEA measurements are a more fitting and robust test of deep dielectric charging codes such as *NUMIT*, as *NUMIT* determines the internal charge distribution to calculate the internal electric field. Experimental validation is particularly important at lower incident electron energies, below 100 keV, where the models for electron penetration depth used in these codes are somewhat less accurate [13,31,32], and can be the most relevant to spacecraft

Presented at the Applied Space Environments Conference 2021, Virtual Event, November 1–5, 2021; received 22 July 2022; revision received 25 October 2022; accepted for publication 27 November 2022; published online 13 February 2023. This material is declared a work of the U.S. Government and is not subject to copyright protection in the United States. All requests for copying and permission to reprint should be submitted to CCC at www.copyright.com; employ the eISSN 1533-6794 to initiate your request. See also AIAA Rights and Permissions www.aiaa.org/randp.

*Ph.D. Candidate, Materials Physics Group, Physics Department; zack.gibson@USU.edu.

[†]Professor, Materials Physics Group, Physics Department; jr.dennison@USU.edu. Senior Member AIAA.

[‡]Professor and Chair, Department of Physics and Engineering; beebri@bethel.edu.

[§]Research Scientist, Space Vehicles Directorate; ryan.hoffmann@us.af.mil.

charging [15]. Fluxes at these lower energies from 10 to 100 keV are much higher in typical space environments [33] and have been shown to lead to most spacecraft anomalies [34].

In this paper, we present a comparison of measurements to simulations for polymers irradiated by mono-energetic electrons. The measurements were made using the PEA method and simulations predicted by *AF-NUMIT3*. The samples chosen to study were polyether-ether ketone (PEEK) and polytetrafluoroethylene (PTFE) as both have very high resistivity so that the embedded charge will be “stationary.” The PEA method utilizes propagating acoustic pressure waves through the sample for measurement. As such, this provides a comparison of results for samples with high acoustic attenuation (PTFE) and low acoustic attenuation (PEEK), as is evident in the results. The incident electron energies chosen were 50 and 80 keV with average beam fluxes of ~ 840 and ~ 640 pA/cm², respectively. The nominal thicknesses of the samples were 125 and 250 μm . Two samples were irradiated at each energy, flux, and thickness in identical conditions to test the reproducibility of the experiment, for a total of 16 samples. The present paper starts by giving a thorough description of the samples and their properties followed by the irradiation details. The results of the experiment and simulations are presented and discussed. The paper ends with conclusions drawn from comparison of the measurements with simulations and a discussion of future work.

II. Experimental Methods

A. Sample Details

PEEK samples from Aptiv Victrex PEEK Film Technology [35] were nominally 125 μm (1000–125G) and 250 μm (1000–250G) thick. PTFE samples from McMaster-Carr were nominally 125 μm (MCVS005X12X3) and 250 μm (SF103V0010) thick. Four samples of each material type and thickness were cut as discs of 3.38 cm diameter. Table 1 lists the samples studied, along with their sample designation and average thicknesses as determined by several measurements with a digital micrometer (Mitutoyo IP65; ± 0.5 μm resolution).

The speed of sound for each sample was determined by dividing the measured thickness by the measured peak-to-peak time difference for the two sample interfaces in the PEA measurements. Estimated aggregate uncertainties were $\sim 0.5\%$ for PEEK and $\sim 3\%$ for PTFE (see Table 2). The primary sources of uncertainties were from the measured

Table 1 Sample ID and thickness

PEEK		PTFE	
ID	Thickness, μm	ID	Thickness, μm
K1A	127.1 \pm 0.8	T1A	128.1 \pm 0.8
K3A	126.1 \pm 0.6	T3A	129.4 \pm 0.9
K4A	126.4 \pm 0.7	T4A	127.0 \pm 0.9
K6A	127.4 \pm 0.7	T6A	129.0 \pm 0.5
K1B	251.0 \pm 0.8	T1B	255.9 \pm 1.2
K3B	248.4 \pm 0.7	T3B	258.1 \pm 1.0
K4B	250.3 \pm 0.7	T4B	256.1 \pm 1.0
K6B	247.8 \pm 0.8	T6B	257.6 \pm 0.9

sample thicknesses ($\lesssim 0.4\%$) and individual sample thickness variations ($\lesssim 1\%$). Uncertainties in the speed of sound at room temperature also include effects from ± 1.5 K temperature variation in the laboratory, estimated to be on the order of $\sim 0.2\%$ [23,36,37]. This uncertainty also depends on the precision and accuracy of the peak-to-peak distance between interfacial peaks in PEA measurements, which have experimental uncertainties on the order of $\sim 10^{-10}$ s or $\lesssim 0.1\%$. There may also be systematic errors resulting from using the peak location instead of the rising edge or an envelope function and from distortions in the peak shapes due to ultrasonic attenuation (especially for PTFE). Sound speeds in polymers are sensitive to chemistry/processing and should be measured for individual samples [37]. The speeds of sound for PEEK and PTFE measured in these studies are in reasonable agreement with literature values [37].

Table 2 lists materials properties for PEEK and PTFE with associated uncertainties; most of these were measured for the specific samples tested at Utah State University (USU). Note that all listed parameters are direct inputs to *AF-NUMIT3* except for the speed of sound and the radiation-induced conductivity (RIC) power (assumed to be unity in *AF-NUMIT3* [13]). Mean atomic numbers and mean atomic weights were calculated as defined in Ref. [22]. The extremely low measured dark conductivities σ_{DC} for PEEK [23] and PTFE [24] coupled with the measured relative permittivity ϵ_r result in decay times $\tau_{DC} \equiv \epsilon_r \epsilon_0 / \sigma_{DC}$ [25] of > 4 months, meaning that deposited charge will be approximately stationary over the timescale of the experiment. Even after several months the charge migration is on the order of < 1 μm ; refer to Ref. [38]. This was an important consideration, as the samples were irradiated at the AFRL facility and then shipped to USU for PEA measurement. The samples were transported and stored in purged, sealed, and light tight containers backfilled with high-purity Ar. Argon storage has been shown to greatly extend recovery times of irradiated polymeric samples, as opposed to exposure to ambient air with moisture or even oxygen or dry nitrogen [39]. During transport, handling, and PEA measurements, cumulative sample exposure to ambient atmosphere was limited to less than ~ 1 h. Likewise, these samples were only exposed to red light to avoid photoconductive charging and discharging, as PEEK has a bandgap at ~ 3.11 eV, just beyond the visible range [40], and exposure to ambient visible or UV light may potentially charge/discharge PEEK samples. The same protocol was followed for PTFE samples, although no photoconductive charging effects were expected.

B. Irradiation Details

Samples were baked out twice before irradiation, once at 100°C for 72 h at $\sim 10^{-4}$ Torr at USU before transport to AFRL, and again at 60°C for 24 h at $\sim 10^{-1}$ Torr at AFRL. Samples were irradiated at room temperature with either 50 or 80 keV using a monoenergetic electron beam (Kimball Physics EGH-8105100 keV electron flood gun) with normal incidence with a vacuum pressure of 8×10^{-7} Torr in the Jumbo chamber at AFRL [41]. Samples were mounted to a 20-cm-OD, 1.3-cm-thick Al disc with two small strips of copper tape (see Fig. 1a). The samples rotated into and out of the beam during irradiation (refer to Fig. 1). In Fig. 1b, the red circles show representative sample positions. The solid black line is the path of the centers of the sample. The dashed black lines outline the active area of the sample to be measured by the PEA system. Beam current is monitored with a Faraday cup at the center of the carousel. The map topology is identical

Table 2 Materials properties

Material	Mean atomic number ^a	Mean atomic weight ^a	Density, ^b g · cm ⁻³	Relative permittivity ^{c,d}	Dark conductivity, ^e S · cm ⁻¹	RIC coefficient, ^{c,f} rad ⁻¹ · s · S · cm ⁻¹	RIC power $\Delta^{c,f}$	Speed of sound, ^c m · s ⁻¹
PEEK	6.12	11.75	1.32 \pm 0.2	3.45 \pm 0.1	(7 \pm 3)e – 21	(2.0 \pm 0.4)e – 16	0.91.1 \pm 0.05	2495 \pm 14
PTFE	8.28	17.25	2.15 \pm 0.2	2.1 \pm 0.1	(2 \pm 3)e – 20	(2.9 \pm 0.6)e – 17	0.98.1 \pm 0.05	1449 \pm 27

^aBased on definition in Ref. [22].

^bManufacturer’s specifications.

^cReferences [1,23].

^dReference [25].

^eReferences [23,24].

^fReferences [24,26].

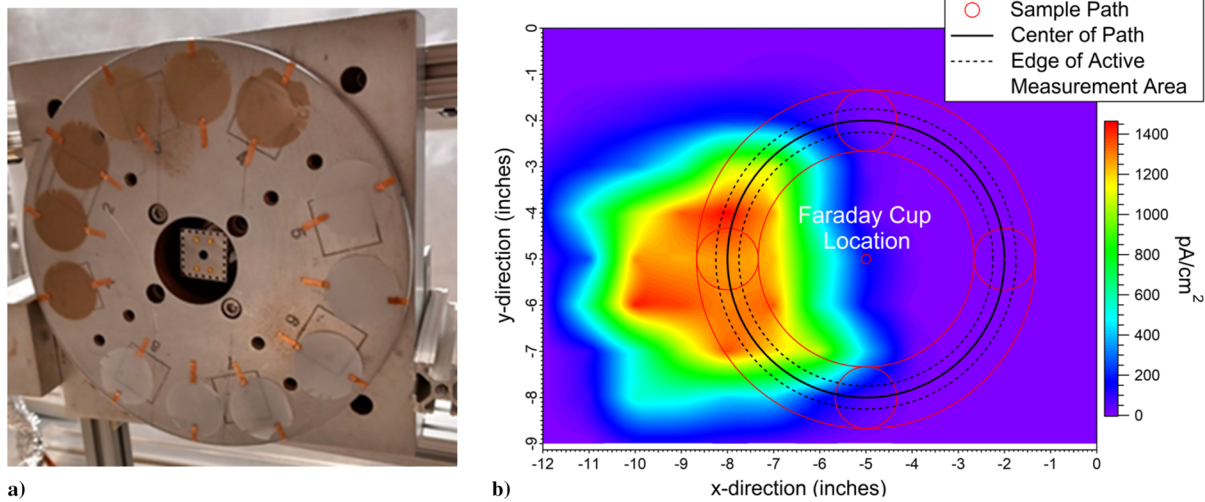


Fig. 1 a) Photograph of one sample set mounted to rotating carousel at AFRL irradiation facilities. The PEEK samples are tan and PTFE samples are white. b) Beam map showing beam current density and the path of the samples through the beam.

for 50 and 80 keV, differing only slightly in amplitude. Pictured is a beam map scaled by a flux of 170 pA/cm² at the Faraday cup. The carousel rotated at 2 RPM for 150 s with the beam on. This gave each sample 75 s cumulative exposure in the beam path in 15 s intervals, as the samples are in the beam path for ~50% of the time due to rotation of the sample stage. The average flux while in the beam path was 840 ± 740 pA/cm² and 640 ± 150 pA/cm², and total fluence was (6.3 ± 5.6) × 10⁻⁴ C/m² and (4.8 ± 1.1) × 10⁻⁴ C/m² for the 50 and 80 keV beams, respectively. Note that there is a large error in the average flux due to the period of higher dose rate near the beginning of the 50 keV irradiation as shown in Fig. 2.

C. PEA Method

There are currently a few different methods for measuring charge distributions in thin dielectrics. PEA measurements are arguably the most promising of several methods for making these measurements for many applications [42]. The other two well-developed methods are pressure wave propagation (PWP) and laser intensity modulation method (LIMM) [1]. A more recently developed method for measuring embedded charge distributions is called electroacoustic reflectometry (EAR) [43]. The advantages to the PEA method are nondestructive measurements, low cost, simplified modeling, and high resolution. For a more in-depth discussion, refer to Dennison and Pearson [1] or Imburgia et al. [44].

The PEA method employed by the USU/Box Elder Innovations PEA system, outlined in Fig. 3, is as follows. An electric field is applied through a pulsed voltage signal (FPG 2-10PM5L high-voltage pulse generator) to a dielectric sample. In this study, the typical pulse is ~0.5 ns in width and ~300 V in amplitude (~3 ns pulse width and

~500 V for some PTFE measurements). This is achieved by setting the pulse generator to 1 kV and using an attenuator (Barth Electronics, Inc., high voltage 8 dB attenuator 142-NMFP-8 B) between the pulse generator and sample. This pulse in turn produces a force on any embedded charge, creating an acoustic pressure wave pulse that propagates through the system and can then be detected by a piezoelectric transducer (9-μm-thick metallized PVDF, Measurement Specialties, Inc., DESC: 9UM/60D/Metalized, 400A Cu/150A Ni, P/N: 1003702-7). The signal is amplified with a low-noise 50 Ω impedance, broadband (9 kHz to 3 GHz) 40 dB gain amplifier (Wenteq ABL0300-00-4030). Simple time-of-flight analysis determines the distribution of charges. In contemporary systems, the dielectric is typically clamped by the cathode and anode [45,46]. The thickness of the samples is on the order of tens to hundreds of micrometers, with diameters on the order of a few centimeters. This means that the method is effectively 1D through the thickness of the film, as the sample can be considered infinitely wide. Note that there is a 500-μm-thick PVC film (McMaster-Carr 87875K17) between the cathode and the sample that is not shown in Fig. 3; this layer is used to improve acoustic coupling in the sample stack [47]. The spatial resolution of the PEA system is defined by the full width at half maximum (FWHM) of the interfacial peak [48], and is approximately 10 μm in the current system. However, the resolution can be affected by sample characteristics such as dispersion and attenuation, as well as the sensor thickness, applied voltage pulse amplitude and duration, and the coupling media used to improve acoustic coupling of materials in the PEA system [49].

In this study, five PEA data sets are recorded, each with 1000 measurements averaged. Statistics are then determined on the five

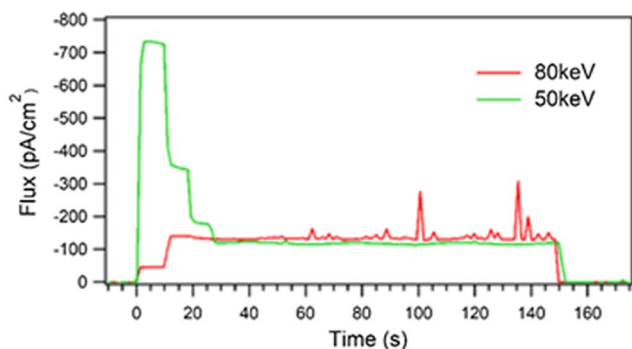


Fig. 2 Electron flux measured with a Faraday cup during irradiation of samples for 50 keV (red) and 80 keV (green) incident energies.

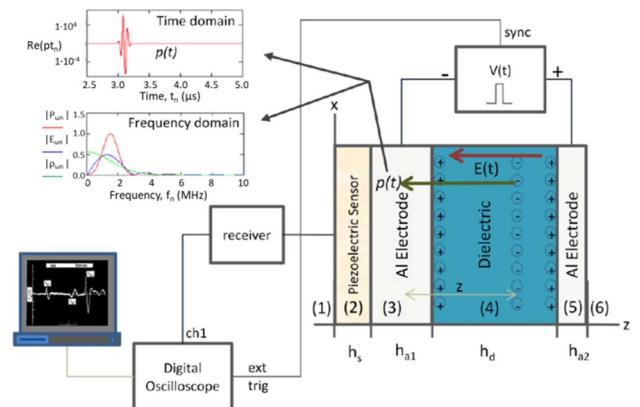


Fig. 3 A conceptual diagram showing a typical PEA system configuration and the electrode/sample/sensor layered structure [1].

data sets to determine several parameters gauging the reproducibility of the measurement, as well as determining the average amplitude versus time signal trace. The averaged data are then processed by applying a modified Gaussian filter, removing the DC offset, and performing a deconvolution via a reference wave to account for system response and to obtain the actual charge distribution. The irradiated samples are measured with no DC bias applied. A reference wave, used for deconvolution and calibration, is obtained by applying a small DC bias between 0.5 and 1 kV using a high voltage direct current (HVDC) power supply (Glassman JF10R12) [50].

Figure 4 shows the data processing sequence for PEA time-domain measurements. Starting with a raw signal (a), a fast Fourier transform (FFT) (b) is taken to determine the filtering parameters used to obtain the filtered time spectra (c). Filtering parameters that can be modified include the center frequency and bandwidth of the filter and noise parameter for deconvolution [51]. Time-domain spectra are converted to distance spectra using the speed of sound measurements described above. A similar measurement is made with a small applied DC bias (0.5–1 kV) (d). The difference between DC bias on and DC bias off spectra is taken to find the system response function (e). This is used for calibration of the measured voltage amplitude in terms of deposited charge. They are further used in the deconvolution process of the original signal; a typical fully processed, filtered, calibrated, and deconvolved spectrum is shown in Fig. 4f.

There are various ways to optimize the signal processing and deconvolution; refer to Fig. 5. We have not corrected for attenuation

and dispersion due to the acoustic signal traveling through the sample; this can be done [52] and is planned for future work. The deconvolution process can be difficult and time-consuming to find optimal parameters to mitigate ringing and artifacts. Optimization procedures exist, and an overview of one method along with the effects of suboptimal deconvolution are given here [53]. There are potential ways to avoid this tedious calibration process [54], but note that the results presented in the present paper have not optimized deconvolution parameters. Other signal processing methods, such as split spectrum processing [51], can be implemented to increase spatial resolution for samples with low acoustic attenuation and dispersion effects, but such processes risk distorting the true signal and potentially decreasing charge density resolution or losing information entirely.

Perturbing the deconvolution and filter parameters can change a number of properties of the final measurement. Some effects include the overall quality of the measurement (ringing and artifacts), peak amplitude of charge distribution, total charge deposited, peak charge deposition depth, width of charge distribution, and asymmetry of charge distribution. Too little filtering results in high noise and overestimation of total charge. Too much filtering results in very low spatial resolution and underestimation of total charge. Approximately optimal deconvolution and filtering results in the most accurate data overall. Examples of these effects are shown in Fig. 5. The largest effects are on signal amplitude, total charge, quality of signal, and spatial resolution. The peak position of the

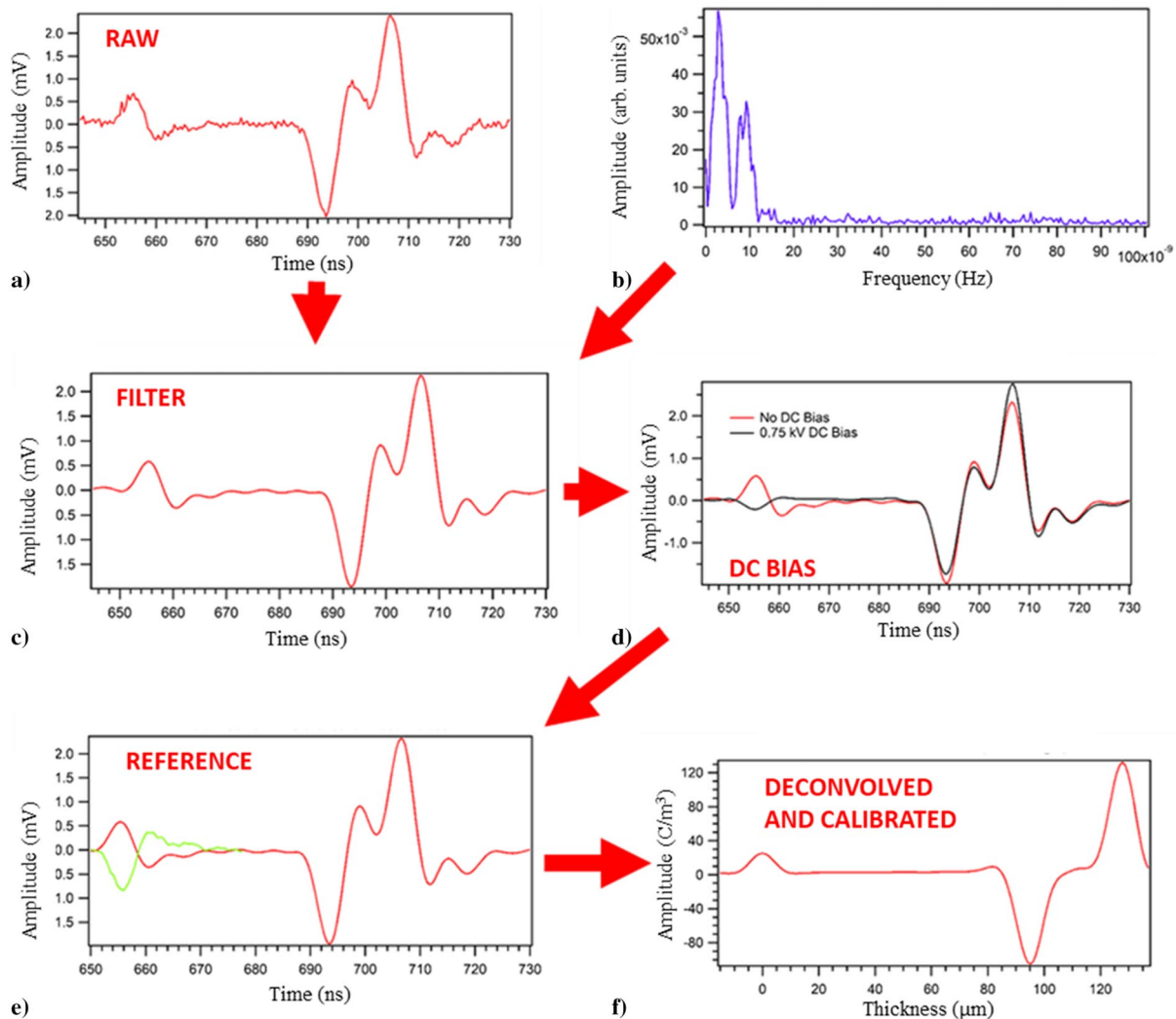


Fig. 4 PEA data processing flowchart: a) raw signal, b) fast Fourier transform (FFT), c) filtered signal, d) DC bias signal for calibration, e) reference signal, and f) deconvolved and calibrated spectra.

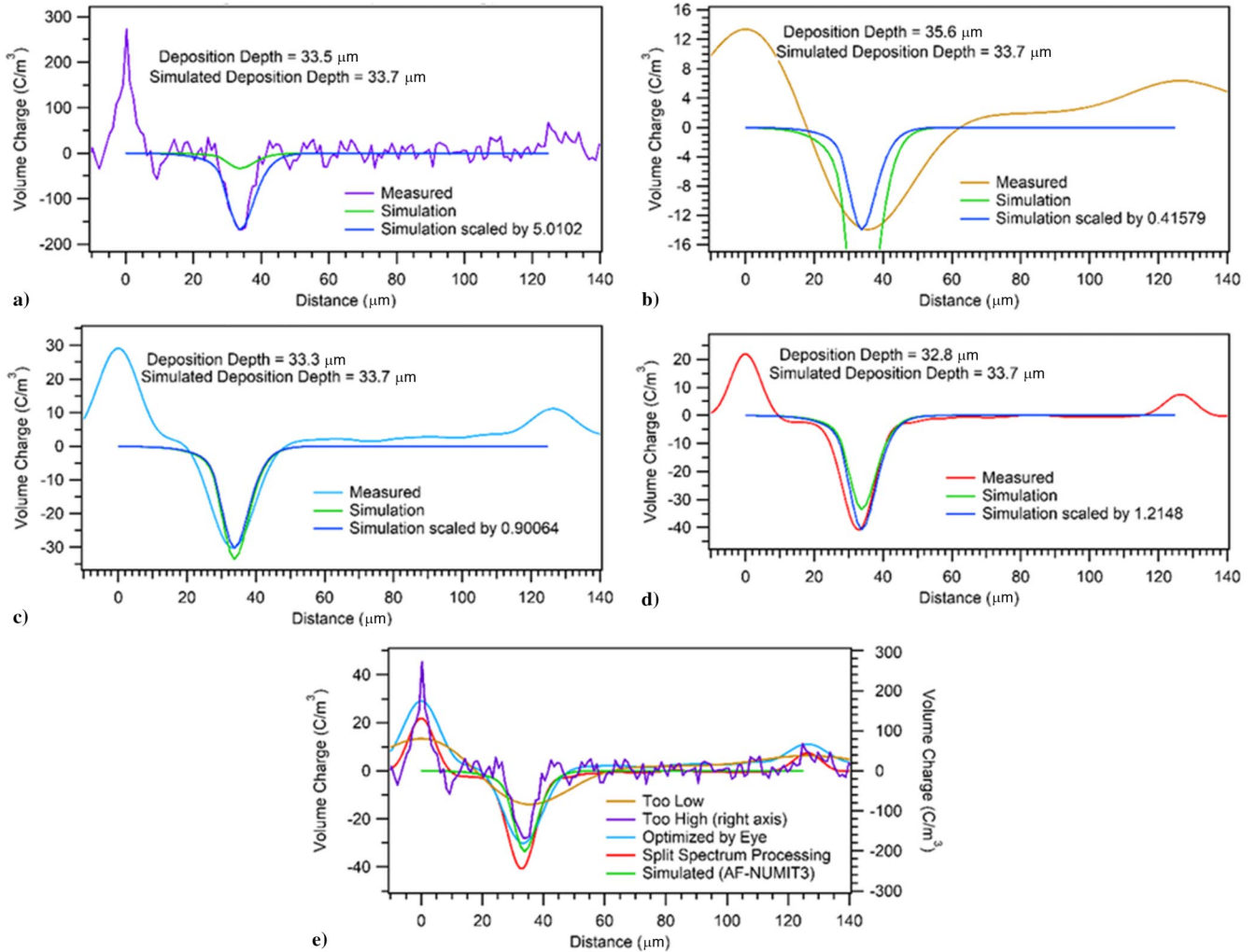


Fig. 5 Effects of filtering on PEA results after deconvolution: a) no filter, b) too much filtering, c) approximately optimized filtering, d) split spectrum processing compared to simulation results, and e) all methods of processing.

charge distribution is largely unaffected, except for very low spatial resolution.

III. Simulation Methods

In the 1970s Frederickson developed a primitive computer model, dubbed *NUMIT* (NUMerical Iteration), designed to correlate experimental observations of charge deposition and transport in dielectric materials with the dynamic situation within the material [17,18]. The 1D model estimated where within the dielectric the electric charge was deposited and the changes to the conductivity of the material resulting from the concomitant deposition of energy (RIC). Then, internal electric fields were calculated, and the resulting movement of charge within the material was predicted. The simulation continued in an iterative fashion using user-defined short time intervals. Since Frederickson's initial idea, numerous other investigators have pursued various improvements to his approach. These include the 1D code *NUMIT 2.1* [15] and a 3D version *NUMIT 3D* [16] adapted by NASA Jet Propulsion Laboratory, and a NUMIT based code developed at Marshal Space Flight Center [55,56]. A number of similar codes mentioned in the Introduction also trace much of their underlying physics principles to the original *NUMIT* work.

Results presented in this paper use *AF-NUMIT3*, a redesign and extension of the original *NUMIT* developed at AFRL by Brian Beecken, used primarily to simulate the space environment [13,14, 57]. Since then, significant further enhancements have been made. *AF-NUMIT3* now allows additional phenomena to be simulated, such

as a moveable/removable front surface electrode, evolving dielectric surface potentials, reduction of incident electron energy due to changing surface potentials, photoemission, and secondary electron emission. In addition, changes in dark conductivity or RIC with time and/or temperature can be modeled. *AF-NUMIT3* can simulate charging both in various laboratory settings (electron beam with normal incidence) and in an approximate space environment (isotropic flux of electrons). The code can handle monoenergetic or broadband sources. Further details of how *AF-NUMIT3* works are described in [13,14,20].

The material inputs to the *AF-NUMIT3* model are listed in Table 2; these are mean atomic number and mean atomic weight from the material composition and stoichiometry, density, relative permittivity, dark (bulk) conductivity, and RIC coefficient. These parameters are all known or measured for the materials studied here. The incident electron flux and energy (normal incidence or isotropic) are also input parameters; modeling here was for monoenergetic normal incidence electron beams.

It is worth noting that the simulations were done before experimentation. That is, there was no fitting to the experimental data in any way. The only "free parameters" in *AF-NUMIT3* are spatial bin size, temporal step size, and a smoothing factor. As is standard practice in simulations, the spatial bin size and temporal step size were chosen so that they had negligible effects on the simulation results while minimizing required computation time. The simulations were all performed with effectively no electrode on the irradiated surface and a grounded electrode on the back surface. Photoemission and secondary electron emission features were not used for this

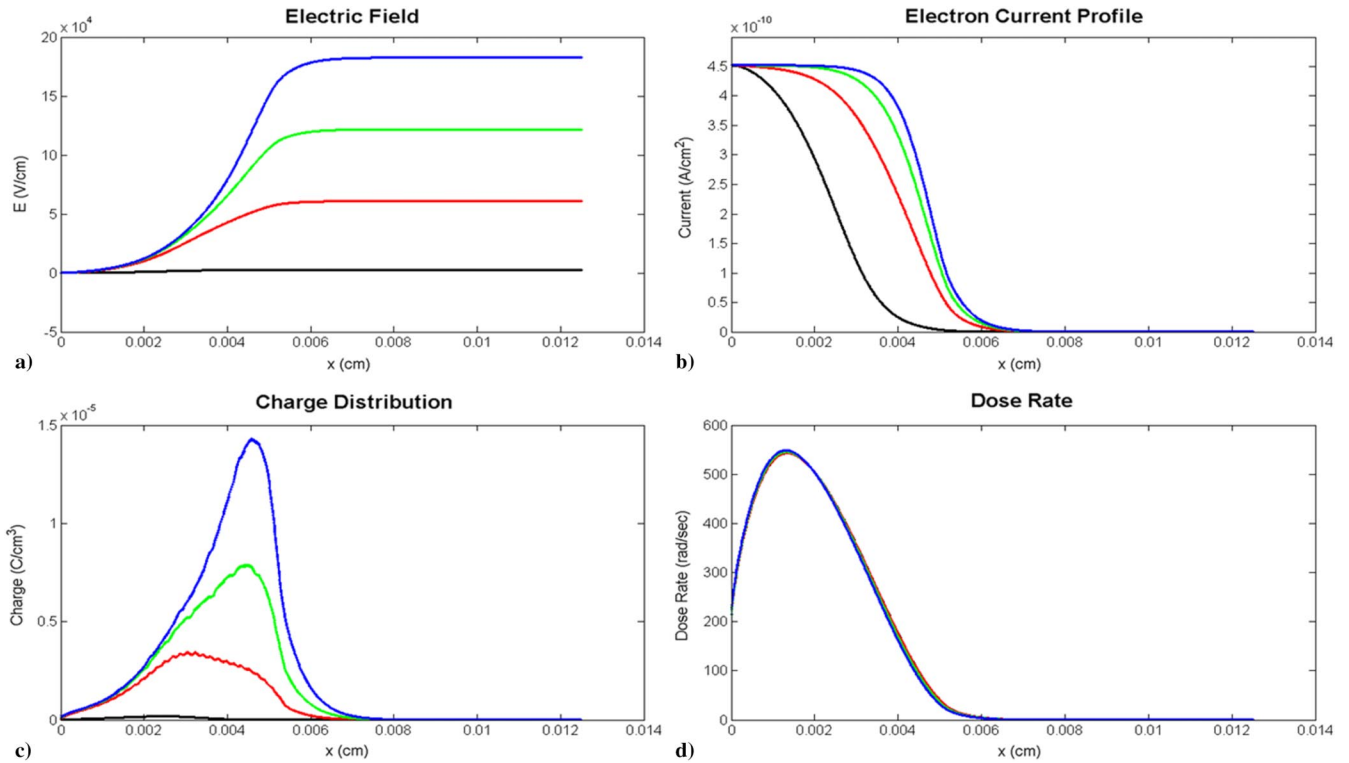


Fig. 6 Typical output plots from AF-NUMIT3: a) internal electric field, b) electron current profile, c) distribution of deposited charge, and d) distribution of deposited energy density (dose rate).

simulation, as they are only important with incident light and low energy ($\lesssim 20$ keV) incident electrons [58], respectively. An example output from AF-NUMIT3 is shown in Fig. 6, which includes the electric field, electron current profile, energy deposition (dose rate) profile, and charge distribution as functions of depth at four sequential time steps. Different times during the irradiation are shown for increasing time in the order black, red, green, and blue. In these graphs, the black lines represent the initial situation immediately after irradiation begins. Note that the electron beam is incident from the left.

In the AF-NUMIT3 simulations the incident beam was approximated by applying the average beam flux for 75 s. Note that this ignores the increased dose for the 50 keV irradiation and slightly decreased dose for 80 keV during the first few seconds of irradiation, as shown in Fig. 2. Also neglected were any delayed or time dependent RIC effects from ramping up/down the beam flux as the sample moves into and out of the center of the beam. Future work is planned to investigate these discrepancies for more accurate predictions.

IV. Results

A. Characterization of Peaks

Figure 7a shows an example of a calibrated plot of charge density versus depth for a typical PEA measurement. In Fig. 7c, a negative charge distribution is deposited in the bulk of the sample when the sample is irradiated with electrons incident from the right. The deposited negative charge induces a positive mirror charge at the interfaces of the electrodes (grey) in the PEA system, denoted with the dashed lines in Fig. 7. These can be seen as positive peaks in the PEA measurement. Interfacial charging of electrodes should reside at the interface surface and therefore highlights the PEA response, showing the spatial resolution of the measurement. Recall that the FWHM of the interfacial peak is considered the spatial resolution of the PEA instrument [47].

To compare the PEA measurements and simulation results, five parameters to characterize the spatial charge profile were extracted from each dataset and compared to results of the simulations. The

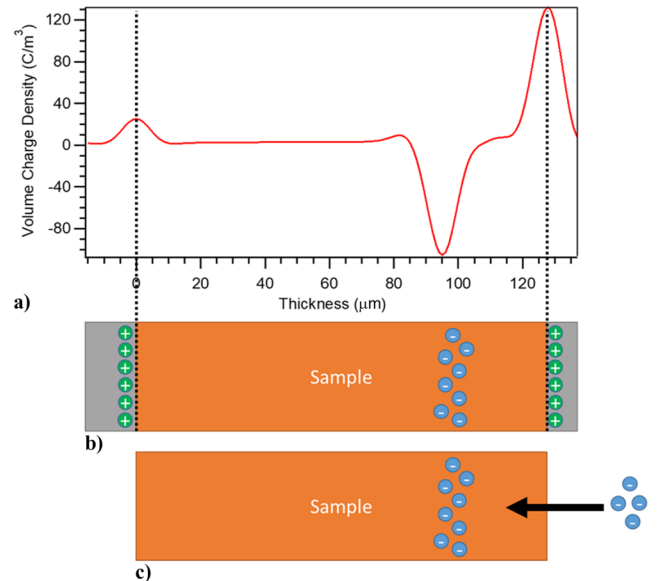


Fig. 7 a) Typical PEA result with schematic representation of b) induced positive mirror charge from c) charge deposited by incident electrons.

integrated area of the charge distribution (total charge deposited per area), the charge distribution peak amplitude, peak deposition depth, FWHM, and half width at half maximum (HWHM) for the two sides of the distribution were determined. These can be directly related to the first four moments about the mean of the embedded charge distribution, that is, the integrated area under the distribution, mean value, standard deviation, and skewness. For example, a symmetric Gaussian distribution, which models the distribution of a thin layer (estimated as ± 1 μm) broadened due to random surface roughness or instrumental effects, is peaked at the mean value and is symmetric about the mean so that the difference between the HWHMs is zero or their ratio is unity (i.e., the first and third moments about the mean are zero).

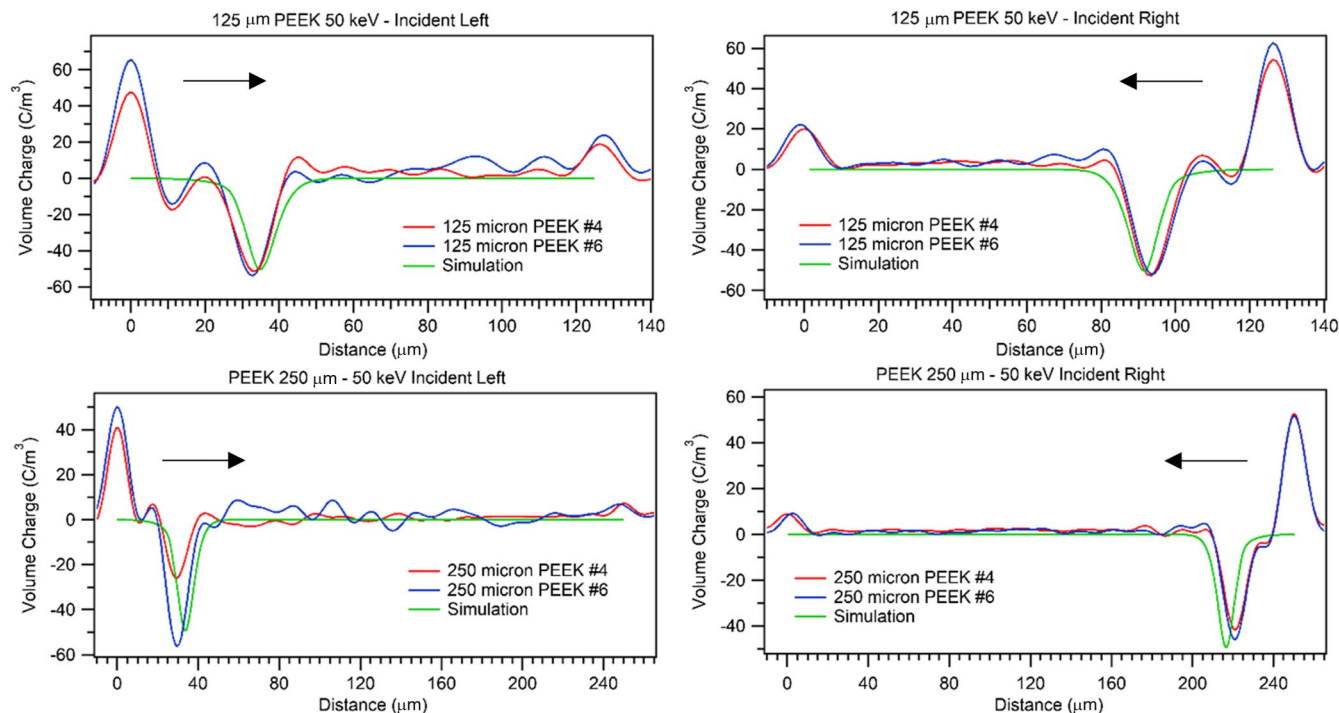


Fig. 8 PEA measurements for 125 μm and 250- μm -thick PEEK samples irradiated with 50 keV electrons are displayed with the AF-NUMIT3 simulations.

Table 3 Characterization of deposited charge distributions for PEEK irradiated with 50 keV electrons

Sample ID	125 μm PEEK					250 μm PEEK				
	Simulation	K4A	K4A	K6A	K6A	Simulation	K4B	K4B	K6B	K6B
Incident direction	Left	Left	Right	Left	Right	Left	Right	Left	Right	Right
Amplitude, $\text{C} \cdot \text{m}^{-3}$	50.2	51.5	52.7	55.9	52.0	49.3	25.9	41.6	56.3	45.9
Deposited charge, $\times 10^{-4} \text{ C} \cdot \text{m}^{-2}$	5.6	5.6	5.7	5.6	5.7	5.6	2.8	5.4	6.9	6.1
Peak depth, μm	34.7	33.2	33.2	32.7	32.6	33.5	29.3	29.2	29.6	29.4
FWHM, μm	9.6	10.8	10.8	10.4	11.0	9.9	10.7	12.4	11.8	12.5
Left HWHM, μm	4.4	5.8	5.3	5.2	5.3	4.9	5.1	6.1	5.7	6.2
Right HWHM, μm	5.2	5.0	5.5	5.2	5.7	5.1	5.6	6.2	6.1	6.4
HWHM ratio	0.9	1.2	1.0	1.0	0.9	1.0	0.9	1.0	0.9	1.0

B. Measured Charge Distributions

Measured and simulated charge profiles for PEEK and PTFE samples irradiated with monoenergetic electrons of 50 and 80 keV incident energies are plotted in Figs. 8–11, with summaries of the peak distribution parameters listed in Tables 3–6. To get an idea of the spatial resolution of each measurement, the FWHM of the leading (left) interfacial peak was determined for each measurement, regardless of the direction of incident charge. The average value of the FWHM is $10.6 \pm 1.1 \mu\text{m}$ and $7.6 \pm 1.5 \mu\text{m}$ for PEEK and PTFE samples, respectively.

Each sample was measured in two orientations as a consistency check, once with the irradiated surface of the sample facing the cathode (pulsing electrode) such that the apparent incident direction is from the right, and once by inverting the sample so that the irradiated surface is facing the anode and the apparent incident direction is from the left. These results should agree, as they are measurements of the same sample in different orientations. Measured curves are aligned to the interfacial peak of the irradiated side, so as to accurately compare deposited charge distributions. This is necessary as samples are of slightly different thicknesses. Samples of differing thickness should also agree, within a few percent, on the deposition depth though there will be some differences in the position of the interfacial peak corresponding to the unirradiated surface due to sample thickness variations.

The left/right incidence measurements are in relatively good agreement for the measurements of PEEK (see Fig. 8). However, this is not the case for PTFE (see Fig. 9). This is to be expected as there are large dispersion and attenuation effects in PTFE.

To obtain an acceptable deconvolution, results for the left incident measurements of 125 and 250 μm PTFE, reference curves from the right incident measurements were used. Measurements of 250 μm PTFE samples 1 and 3 were unable to be accurately calibrated for volume charge. A poor calibration was obtained for the right incident measurements, and the left incident measurements use the reference curves from the right incident measurements, so no attempt of charge magnitude calibration was made for the left incidence. Left incident measurements of 125 μm PTFE samples 4 and 6 were unable to be accurately calibrated for volume charge as well. The right incident measurement of 125 μm PTFE sample 6 had to be calibrated using the sample 4 reference curve. All other samples were calibrated in a typical manner as outlined in the *PEA Method* section.

The integrated area of the charge distributions can be used as a consistency check by comparing it to the total expected fluence. The units of the integrated charge distributions are C/m^2 , that is, charge per unit area. As the measurements are 1D in nature, it is reasonable to express charge density or fluence in terms of charge per unit area. The total fluences expected based on the experimental incident electron fluxes are approximately 6.4×10^{-4} and $4.8 \times 10^{-4} \text{ C}/\text{m}^2$ for 50 and

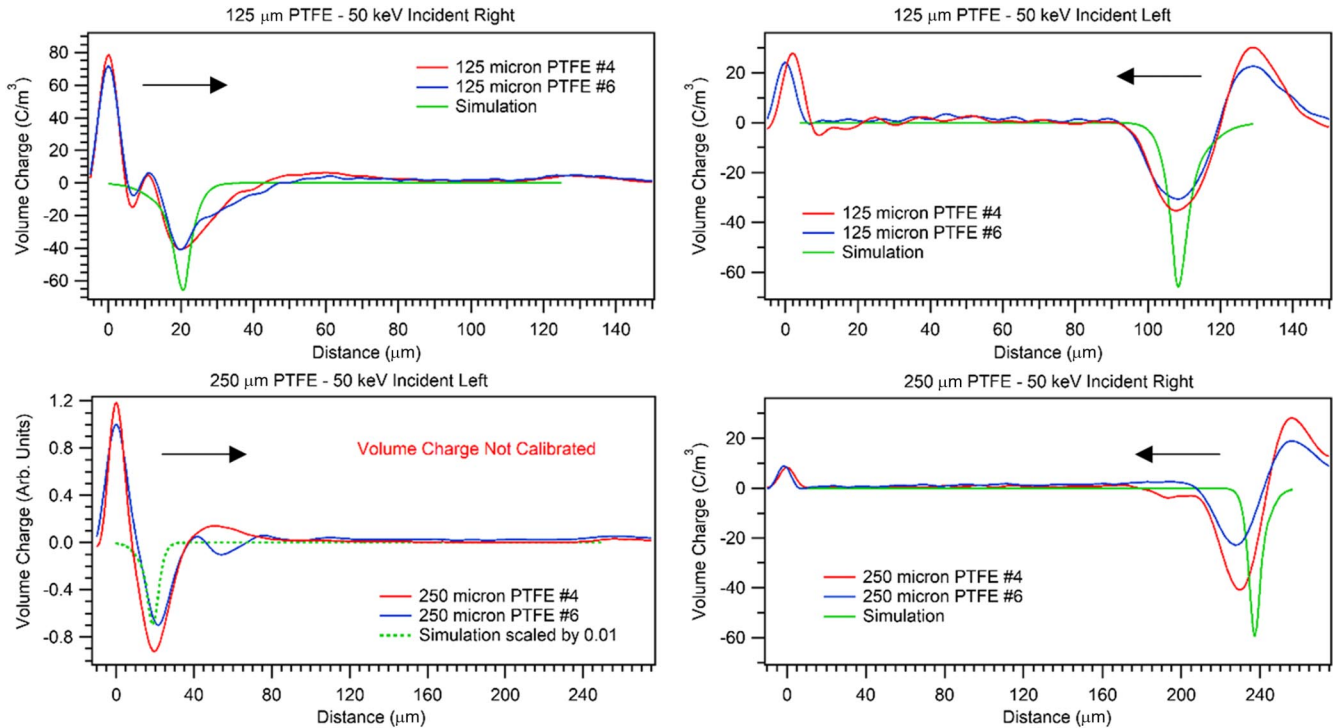


Fig. 9 PEA measurements for 125 μm and 250- μm -thick PTFE samples irradiated with 50 keV electrons are displayed with the AF-NUMIT3 simulations.

Table 4 Characterization of deposited charge distributions for PTFE irradiated with 50 keV electrons

Sample ID	125 μm PTFE					250 μm PTFE				
	Simulation	T4A	T4A	T6A	T6A	Simulation	T4B	T4B	T6B	T6B
Incident direction	Left	Left	Right	Left	Right	Left	Left	Right	Left	Right
Amplitude, $\text{C} \cdot \text{m}^{-3}$	65.8	40.6	35.3	41.1	30.7	59.5	0.9 ^a	32.6	0.7 ^a	22.8
Deposited charge, $\times 10^{-4} \text{C} \cdot \text{m}^{-2}$	5.3	6.1	5.6	5.8	5	5.3	0.15 ^a	6.1	0.1 ^a	4.5
Peak depth, μm	20.6	20.1	21.2	20	20.8	18.9	19.6	26.4	21.6	28.4
FWHM, μm	6.0	14.5	16.3	11.8	16.9	7.1	16.0	19.0	13.9	20.0
Left HWHM, μm	3.5	5.1	7.5	3.9	8.8	3.7	7.3	10.4	6.6	10.8
Right HWHM, μm	2.6	9.4	8.7	7.9	8.0	3.4	8.7	8.6	7.3	9.2
HWHM ratio	1.3	0.5	0.9	0.2	1.1	1.1	0.8	1.2	1.0	1.2

^aNot accurately calibrated for volume charge.

80 keV irradiations, respectively. Note that $\sim 10\%$ backscatter is typical for these higher incident energy electrons and was assumed for comparison to measurements. The total fluence was determined for a PEA measurement by integrating over the deposited charge distribution (ignoring induced charge on electrodes).

For 50 keV irradiated PEEK samples the fractional differences between predicted and measured total fluence are 4 and 29% for the 125 and 250 μm samples, respectively. Ignoring the uncalibrated data for 50 keV irradiated PTFE, these fractional differences are 8 and 19% for 125 and 250 μm samples, respectively. Thus, both the PTFE and PEEK are in relatively good agreement with predicted charge deposition, considering the potential error introduced with signal processing.

The 80 keV irradiated samples (see Figs. 10 and 11) exhibit much poorer agreement. The thinner PEEK sample data exhibit a significant discrepancy in total charge deposited. Several repeated measurements indicate that this is not a calibration issue. It is unclear where this charge in excess of the prediction came from. The thicker PEEK samples (see Fig. 10) have a relatively smaller discrepancy in deposited charge of $\sim 55\%$. The thicker PEEK samples also appear to exhibit a positive charge distribution between the deposited negative distribution and the irradiation surface; more investigation is required to confirm if this positive distribution is real or an artifact of signal processing.

Some of the most interesting results are obtained from the 80 keV irradiated PTFE samples (see Fig. 11), which exhibit multiple peaks in the measured deposited charge distributions. For all 80 keV PTFE samples, there is a negative peak near the irradiated surface and another negative peak much deeper in the sample. The 250 μm PTFE samples also show a possible positive charge peak between the two negative charge peaks, which could be due to deconvolution artifacts. Ignoring the uncalibrated measurements, the fractional differences in the total charge (totaled for all distributions in a sample of 80 keV irradiated PTFE) is 43 and 80% for the 125 and 250 μm samples, respectively.

The uncertainty in the peak deposition depth for PEEK is $\leq 0.5 \mu\text{m}$. The PEA measurements for the different thickness samples are in good agreement for the 80 keV data, but not for the 50 keV data. The discrepancy in peak deposition depth in the 50 keV measurements between the two thicknesses is thought to be related to the 125- μm -thick samples receiving a significantly higher dose rate during the beginning of the irradiation. Figure 2 shows a period of higher flux at the beginning of the 50 keV irradiation that was only incident on some of the samples as the samples are rotated into and out of the beam; refer to Fig. 1.

The uncertainty in the peak deposition depth for PTFE is $\leq 2 \mu\text{m}$. This uncertainty could be decreased by decreasing the uncertainty in the speed of sound. However, this process is complicated

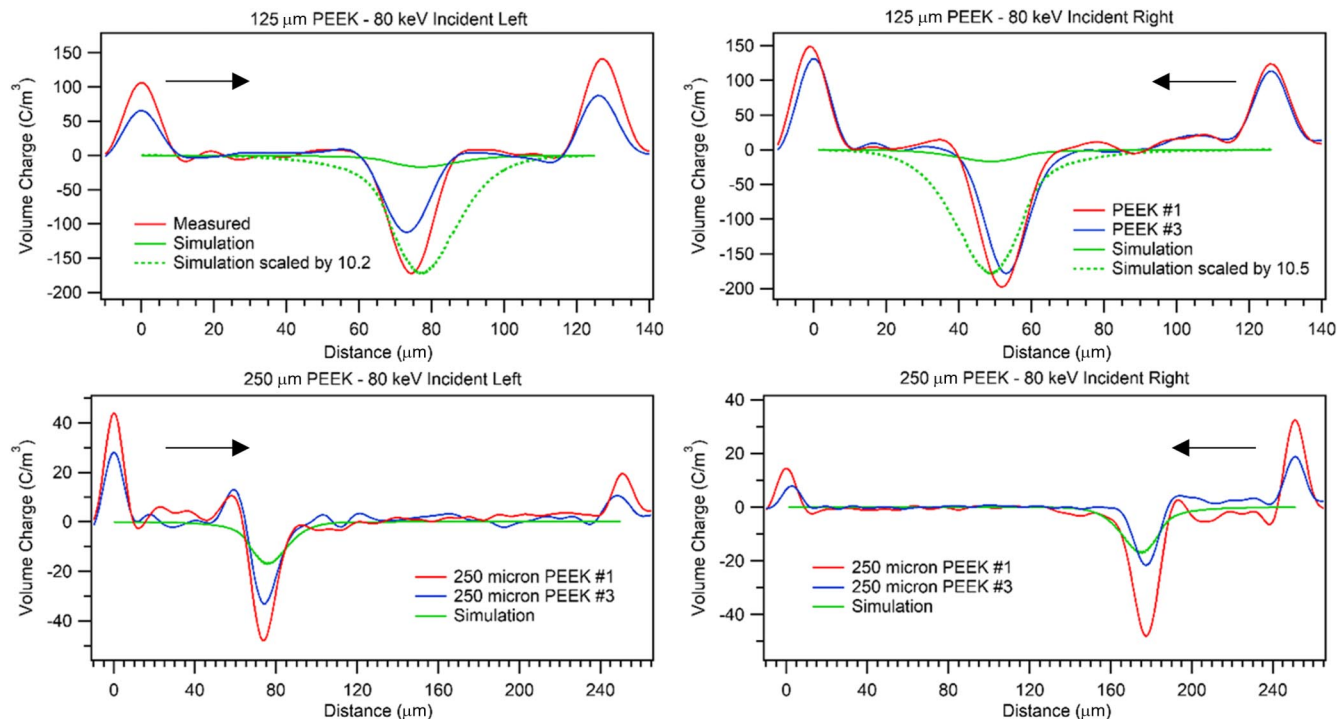


Fig. 10 PEA measurements for 125 μm and 250- μm -thick PEEK samples irradiated with 80 keV electrons are displayed with the AF-NUMIT3 simulations.

Table 5 Characterization of deposited charge distribution for PEEK irradiated with 80 keV electrons

Sample ID	125 μm PEEK					250 μm PEEK				
	Simulation	K1A	K1A	K3A	K3A	Simulation	K1B	K1B	K3B	K3B
Incident direction	Left	Left	Right	Left	Right	Left	Left	Right	Left	Right
Amplitude, $\text{C} \cdot \text{m}^{-3}$	17.0	172.6	198.2	112.3	178.6	16.8	48.0	48.1	33.1	21.6
Deposited charge, $\times 10^{-4} \text{C} \cdot \text{m}^{-2}$	4.3	24	28	16	27	4.3	7.3	8.2	4.8	2.9
Peak depth, μm	77.3	74.4	74.3	73.2	73	75.1	73.8	73.5	74.3	73.5
FWHM, μm	21.1	13.5	13.9	14.1	13.8	21.4	13.3	14.9	13.9	13.2
Left HWHM, μm	9.7	7.0	6.9	7.1	6.8	9.1	6.2	7.9	6.1	6.9
Right HWHM, μm	11.4	6.6	7.0	7.0	7.0	12.3	7.1	7.0	7.8	6.4
HWHM ratio	0.9	1.1	1.0	1.0	1.0	0.7	0.9	1.1	0.8	1.1

by large differences when comparing the left/right incidence measurements, due mostly to the large acoustic attenuation and dispersion effects for PTFE. The deposition depths measured for left incidence are more accurate, as the attenuation and dispersion effects are minimized because the signal travels through less sample material.

Note that the skewness, as gauged by the half-width-half-maximum ratios (see Tables 3–6), can also change with perturbation of processing parameters. The PEEK samples of both irradiation energies have essentially no asymmetry (a ratio of ~ 1). PTFE samples show asymmetry in measurements that are not consistent between left/right incidence measurements. This could be due to the dispersion and attenuation effects. Further investigation is needed to more accurately characterize the asymmetry of PEA measurements through comparison of asymmetries of the interfacial peaks for raw and processed data.

C. Simulated Charge Distributions

The AF-NUMIT3 simulation results were also characterized by the deposited peak characteristics, as outlined in the previous section.

The total charge deposited in the sample for the simulations is less than the expected total fluence from experimental fluxes by $\sim 10\%$.

This is due to a backscatter term used in the simulation code; refer to Eq. (8) in [59]. This same backscatter correction is used for all the simulations, and the total deposited charge is the same for different thicknesses in the various simulations.

However, the amplitude and position of the deposited charge distribution is predicted by the simulations to be slightly different for different thicknesses. The amplitudes and peak deposition depths are lower for the 250- μm -thick samples than 125- μm -thick samples. However, these effects are relatively small, differing by only a few percent. These effects are likely due to RIC in the irradiated region during irradiation, which can persist for some time after irradiation due to delayed RIC. There is no electrode at the front surface and hence no potential difference or electric field between the deposited charge distribution and the front surface driving charge transport in the irradiated region. However, a mirror charge induced on the rear grounded surface of the sample carousel due to the deposited charge distribution causes an electric field proportional to the distance between the deposited charge distribution and the rear electrode. Thus, there will be a stronger electric field for thinner samples with reduced distance to the rear grounded surface than for thicker counterparts. RIC effects increase the conductivity enough for the charge in the irradiated region to be somewhat mobile during irradiation. This will allow the electric field to drive the peak of the charge

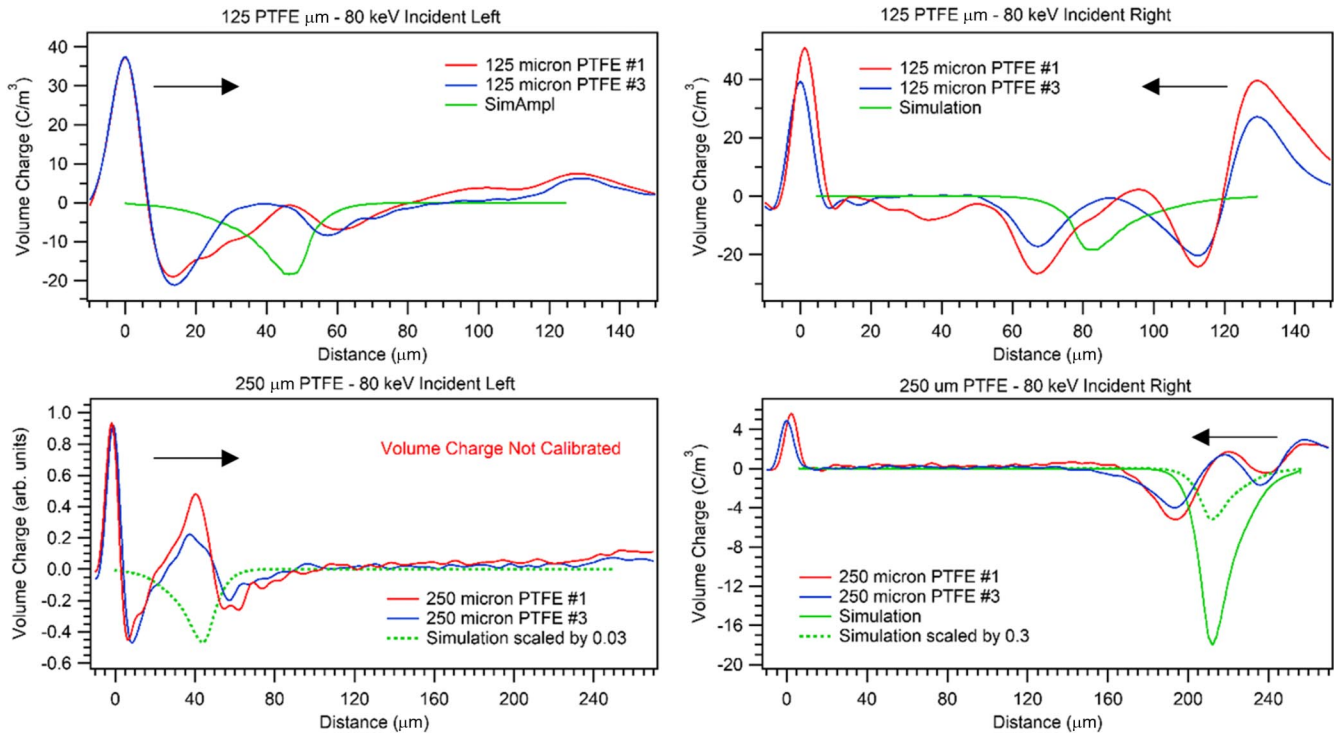


Fig. 11 PEA measurements for 125 μm and 250- μm -thick PTFE samples irradiated with 80 keV electrons are displayed with the AF-NUMIT3 simulations.

Table 6 Characterization of deposited charge distribution for PTFE irradiated with 80 keV electrons

Sample ID	250 μm PTFE													
	Simulation	T1B	T1B	T1B	T1B	T1B	T1B	T1B	T3B	T3B	T3B	T3B	T3B	
Incident direction	Left	Left	Left	Left	Right	Right	Right	Right	Left	Left	Left	Right	Right	Right
Amplitude, $\text{C} \cdot \text{m}^{-3}$	18.0	0.5 ^a	0.5 ^a	0.3 ^a	0.5 ^a	1.7 ^a	5.2 ^a	0.2 ^a	0.5 ^a	0.2 ^a	1.7 ^a	1.4 ^a	4.0 ^a	
Deposited charge, $\times 10^{-4} \text{C} \cdot \text{m}^{-2}$	4.0	0.05 ^a	0.07 ^a	—	0.04 ^a	0.24 ^a	1.2 ^a	0.03 ^a	0.05 ^a	0.03 ^a	0.18 ^a	0.17 ^a	0.45 ^a	
Peak depth, μm	43.7	6.7	40.4	54.9	18.9	37.9	64.5	37.5	8.6	57.2	22.1	39.7	64.9	
FWHM, μm	18.4	11.0	12.8	15.9	8.2	14.6	22.5	14.1	9.8	10.0	11.2	12.1	22.8	
Left HWHM, μm	11.1	2.6	7.1	3.9	4.8	6.9	12.4	5.2	3.3	4.2	5.3	6.4	13.7	
Right HWHM, μm	7.3	8.4	5.7	12.0	3.5	7.7	10.1	8.9	6.5	5.8	5.8	5.7	9.1	
HWHM ratio	1.5	0.3	1.3	0.3	1.4	0.9	1.2	0.6	0.5	0.7	0.9	1.1	1.5	
Sample ID	125 μm PTFE													
	Simulation	T1A	T1A	T1A	T1A	T3A	T3A	T3A	T3A	T3A				
Incident direction	Left	Left	Left	Right	Right	Left	Left	Right	Right					
Amplitude, $\text{C} \cdot \text{m}^{-3}$	18.3	6.9	19.0	26.4	24.1	8.4	21.1	17.1	20.3					
Deposited charge, $\times 10^{-4} \text{C} \cdot \text{m}^{-2}$	4.0	1.3	4.2	4.9	2.7	1.7	3.1	2.8	3.3					
Peak depth, μm	45.5	60.6	13.6	62.2	16.8	57.4	14	62.2	17					
FWHM, μm	16.9	17.4	23.2	16.6	11.5	15.9	14.7	15.1	15.9					
Left HWHM, μm	9.8	7.7	5.4	7.2	6.6	6.7	5.4	6.9	10.3					
Right HWHM, μm	7.2	9.7	17.8	9.5	4.9	9.1	9.3	8.1	5.6					
HWHM ratio	1.4	0.8	0.3	0.8	1.3	0.7	0.6	0.9	1.9					

^aNot accurately calibrated for volume charge.

distribution deeper into the sample. The effect of this is seen as a deeper peak deposition depth approaching the range of the irradiating electron flux and a higher amplitude peak as the charge tries to accumulate as deep as the dose (and therefore RIC effects) penetrate.

The simulations also predict an asymmetry in the deposited charge distributions. The asymmetry differs slightly for differing thicknesses as well, which is also likely explained by RIC effects described above. For PEEK samples, the charge distribution is skewed such that the distribution is wider deeper into the dielectric (away from the incident surface). The opposite is true for the PTFE simulations; the charge distribution is skewed toward the incident surface. Such

differences may also be a reflection of a more complex spatial distribution of charge carriers (perhaps both electrons and holes).

V. Discussion

The results of the PEA measurements and simulations have been summarized. This section compares the PEA measurements with the AF-NUMIT3 simulations and comments on their agreement based on the characteristics of the deposited charge distributions.

The amplitude of any given charge distribution is not a good measure of accuracy, as this will change with the resolution and

processing of the data. Note that the total charge is also not a good comparison, as the PEA calibration methods and data processing have not been optimized. However, even with suboptimal processing, we expect the magnitude of the charge distribution and total deposited charge to agree between simulation and experiment to within a factor of a few or better.

The *AF-NUMIT3* simulations agree well with the 50 keV irradiated PEEK samples. The peak deposition depth for the 125- μm -thick PEEK was within 5% of the average PEA measurement. The results for the 250- μm -thick sample were not as good, but still fell within 12%. However, it seems likely that the 125 μm PEEK samples were irradiated with the higher dose at the beginning of irradiation, as seen in Fig. 2. That change in irradiation was not included in the *AF-NUMIT3* simulation predictions. It is also possible that the difference in agreement is a thickness effect. As discussed in the previous section, RIC allows charge to be somewhat mobile during irradiation. Delayed RIC would continue operating between the irradiation periods, and the *AF-NUMIT3* simulation prediction did not account for that. Further investigation is needed.

The 80 keV irradiated PEEK PEA results, however, do not seem to corroborate the argument that it could be due to differences in thickness. The simulation peaks are at a depth that falls within 5% of the average PEA measurement for the 125 μm samples and within 2% for the 250 μm samples. The measured deposition depth disagrees with the simulated deposition depth, by being 1–3 μm shallower, depending on the thickness of the sample (deeper for thinner sample). Taking into account the large errors with the amplitude and total charge deposited for the PEA measurements, the simulation results, by almost all parameters, are in relatively good agreement for PEEK at both 50 and 80 keV incident energies (aside from K1A and K3A, which have inexplicably large amounts of charge).

The simulations did not predict a significant asymmetry in the embedded charge distribution, and no significant asymmetry was measured for the PEEK data, except for the thicker 80 keV irradiation, which was predicted and measured. Note that the narrow distributions are likely due to RIC effects, and the slight discrepancy in the degree of asymmetry in the thicker 80 keV PEEK samples may be due to delayed RIC not taken into account by the simulation. Delayed RIC is the residual RIC that decays after the radiation has stopped. This could potentially drive the charge deeper into the sample because the conductivity is elevated due to delayed RIC. RIC is dose dependent, so charge will be unable to travel deeper than the range of the incident dose. This results in a narrower distribution that is peaked slightly deeper than the original deposited distribution. Delayed RIC is an option that can be modeled using *AF-NUMIT3*, but was not utilized here, as the incident beam was modeled as a continuous irradiation using a constant (average) flux.

The width of the distributions for the 80 keV irradiated PEEK samples, as determined by the FWHM, is also narrower than the simulated charge distributions. This supports the delayed RIC argument. However, the FWHMs are essentially as predicted for the 50 keV irradiated PEEK samples. This could be due to spatial resolution of the PEA system. Therefore, the actual charge distribution may be narrower than can be determined by PEA measurements. Higher spatial resolution measurements would be necessary to investigate this. The delayed RIC portion of the *AF-NUMIT3* code should be tested against such data in the future. Note that there also appears to be a slight positive charge peak in the 250 μm 80 keV irradiated PEEK measurements. Here we are focusing only on the large negative charge peak for comparison to *AF-NUMIT3*.

PTFE data are much harder to deal with and to compare to the *AF-NUMIT3* simulations. Several measurements were unable to be calibrated for volume charge, so the magnitude of charge cannot be compared to simulations. The 50 keV irradiated PTFE measurements agree with the simulations quite well for the peak deposition depth with five of six measurements within one micron. There is less agreement with the right incident 250 μm samples, likely due to the high attenuation and dispersion. The measured peaks are wider than the simulations by approximately a factor of 2. This is likely due to lower spatial resolution in PTFE samples. The asymmetry of the charge distributions is predicted to be broader toward the irradiated

surface, but the measurements appear to exhibit a broader distribution deeper into the sample.

For 80 keV irradiated PTFE there is poorer agreement between measurement and simulation. PTFE is very hard to keep uncharged, so it is possible that there was surface charge on the samples before irradiation began. The samples were stored and handled carefully, and underwent vacuum bake out in an attempt to minimize residual charge. It is also possible that material damage played a role, as the onset of damage in PTFE is a total ionizing dose (TID) of $\sim 10^4$ rad [60,61] and the TID received here is $\sim 10^4$ – 10^5 rad.

It should be noted that dual negative peaks have previously been measured in electron irradiated PTFE [62], as well as in other USU laboratory unpublished data. In Ref. [62], the dual negative peaks appeared when the charge distribution was measured using what they termed “short circuit PEA,” which is essentially equivalent to the approach in the present paper. The authors of Ref. [62], however, also did the same experiment with an “open PEA” system. Using that approach produced one negative peak that has been precisely replicated with *AF-NUMIT3* in Ref. [19]. Work needs to be done to determine how the different irradiation environments and/or PEA systems produce such, as well as investigating irradiation with lower energy electrons [63].

As the deposited distributions differ substantially from the simulated charge distributions in a quantitative comparison, it makes little sense in comparing the rest of the details of the simulation. However, it is perhaps worth noting that the FWHM of the simulations is larger than the measured FWHM of the deposited peaks for almost all 80 keV 250 μm PTFE measurements. The one exception is the deepest deposited peak in sample T3B. The FWHM is closer to agreement for samples T1A and T3A, but still differs by several microns.

VI. Conclusions

This paper has presented a detailed comparison of PEA measurements and *AF-NUMIT3* simulations for PEEK and PTFE samples irradiated with 50 and 80 keV monoenergetic electrons. The overall agreement of the simulations with experiment is very encouraging. However, there are several areas that can be improved upon.

Improvement to PEA measurements can be accomplished through optimization of PEA calibration and data processing methods for a more accurate comparison. In particular, this includes optimizing the filtering and deconvolution of data and taking into account the dispersion and attenuation effects of the sample. Better and more fully characterized spatial resolution of PEA systems would also be advantageous.

A potential improvement to the simulations is to better model time-varying incident fluxes. The results described here are an excellent example for such a more refined model, as the incident electron beam varied over the course of irradiation and the flux incident on the sample varied further as the samples moved in and out of the beam during irradiation. Inclusion of delayed RIC effects is likely to become important under such circumstances, as conductivity then becomes time dependent. These effects are a topic of future work for the authors.

The agreement between simulations and measurements here is very promising. Future work should include addressing the improvements mentioned above and comparing PEA measurements to other models such as the JPL version of *NUMIT*, pushing the PEA system to measure polymers irradiated with even lower incident energies that are particularly relevant to spacecraft charging (this work is underway [63]), and studying the effects of the presence or absence of surface electrodes during irradiation for both experiments and simulations.

Acknowledgments

This research was supported in part by the Air Force Research Laboratory, Space Vehicles Directorate, through the Air Force Office of Scientific Research Summer Faculty Fellowship Program[®], Contract Numbers FA8750-15-3-6003, FA9550-15-0001 and FA9550-20-F-0005. This work was partially supported by Small Business Technology Transfer Research (STTR) Phase I and Phase II funding

from the Air Force Research Laboratory, Kirtland Air Force Base, Albuquerque, New Mexico. Gibson acknowledges support through a Presidential Doctoral Research Fellowship from the Utah State University Office of Research. L. H. Pearson, E. W. Griffiths, and A. C. Pearson of Box Elder Innovations, LLC, were instrumental in the development of the pulsed electroacoustic test system used for the pulsed electroacoustic measurements.

Disclaimer

The views expressed are those of the authors and do not reflect the official guidance or position of the United States Government, the Department of Defense, or of the United States Air Force.

Statement from Department of Defense: The appearance of external hyperlinks does not constitute endorsement by the United States Department of Defense (DoD) of the linked websites, or the information, products, or services contained therein. The DoD does not exercise any editorial, security, or other control over the information you may find at these locations.

References

- [1] Dennison, J. R., and Pearson, L. H., "Pulsed Electro-Acoustic (PEA) Measurements of Embedded Charge Distributions," *Proceedings of SPIE 887612, Nanophotonics and Macrophotonics for Space Environments VII*, Sept. 2013.
<https://doi.org/10.1117/12.2025667>
- [2] Hussaini, H., Adam, A. A., and Susan, A. A., "Review of Space-Charge Measurement Using Pulsed Electro-Acoustic Method: Advantages and Limitations," *International Journal of Engineering Research and Applications*, Vol. 5, No. 4, 2015, pp. 90–95.
- [3] Garrett, H. B., and Whittlesey, A. C., "Spacecraft Charging, an Update," *IEEE Transactions on Plasma Science*, Vol. 28, No. 6, Dec. 2000, pp. 2017–2028.
<https://doi.org/10.1109/27.902229>
- [4] Leach, R. D., and Alexander, M. B., *Failures and Anomalies Attributed to Spacecraft Charging*, Vol. 1375, NASA, Marshall Space Flight Center, Huntsville, AL, 1995, pp. 2–17.
- [5] Ferguson, D. C., Worden, S. P., and Hastings, D. E., "The Space Weather Threat to Situational Awareness, Communications, and Positioning Systems," *IEEE Transactions on Plasma Science*, Vol. 43, No. 9, 2015, pp. 3086–3098.
<https://doi.org/10.1109/TPS.2015.2412775>
- [6] Bedingfield, K. L., and Leach, R. D., *Spacecraft System Failures and Anomalies Attributed to the Natural Space Environment*, Vol. 1390, NASA, Marshall Space Flight Center, Huntsville, AL, 1996, pp. 1–6.
- [7] Pacaud, R., Paulmier, T., Sarrailh, P., Ryden, K., Hands, A., and Payan, D., "Study of Internal Charging of Four Commonly Used Polymers Through Experimental and Numerical Analysis," *Journal of Applied Physics*, Vol. 125, No. 4, 2019, Paper 045108.
<https://doi.org/10.1063/1.5055221>
- [8] Lei, F., Rodgers, D., and Truscott, P., "MCICT—Monte Carlo Internal Charging Tool," *14th Spacecraft Charging Technology Conference, ESA/ESTEC*, Vol. 4, No. 8, Noordwijk, NL, April 2016.
- [9] Sorensen, J., Rodgers, D., Ryden, K., Latham, P., Wrenn, G., Levy, L., and Panabiere, G., "ESA's Tools for Internal Charging," *1999 Fifth European Conference on Radiation and Its Effects on Components and Systems, RADECS 99 (Cat. No. 99TH8471)*, Inst. of Electrical and Electronics Engineers, New York, 1999, pp. 27–33.
<https://doi.org/10.1109/RADECS.1999.858540>
- [10] Rodgers, D. J., Ryden, K. A., Wrenn, G. L., Latham, P. M., Sorensen, J., and Levy, L., "An Engineering Tool for the Prediction of Internal Dielectric Charging," *6th Spacecraft Charging Technology Conference*, 1998.
- [11] Agostinelli, S., Allison, J., Amako, K. A., Apostolakis, J., Araujo, H., Arce, P., Asai, M., Axen, D., Banerjee, S., Barrand, G. J. N. I., and Behner, F., "GEANT4—A Simulation Toolkit," *Nuclear Instruments and Methods in Physics Research Section A: Accelerators, Spectrometers, Detectors and Associated Equipment*, Vol. 506, No. 3, 2003, pp. 250–303.
[https://doi.org/10.1016/S0168-9002\(03\)01368-8](https://doi.org/10.1016/S0168-9002(03)01368-8)
- [12] Yu, X. Q., HongFei, C., QiuGang, Z., JianZhao, W., WeiHong, S., Hong, Z., JiQing, Z., WeiYing, Z., Zhe, C., SiPei, S., and XianGhong, J., "Leakage Current of Grounded Dielectrics in Electron Radiation as a Diagnostic Method to Evaluate the Deep Charging Hazards in Space," *IEEE Transactions on Nuclear Science*, Vol. 63, No. 2, 2016, pp. 1306–1313.
<https://doi.org/10.1109/TNS.2016.2537839>
- [13] Beecken, B. P., Englund, J. T., Lake, J. J., and Wallin, B. M., "Application of AF-NUMIT2 to the Modeling of Deep-Dielectric Spacecraft Charging in the Space Environment," *IEEE Transactions on Plasma Science*, Vol. 43, No. 9, 2015, pp. 2817–2827.
<https://doi.org/10.1109/TPS.2015.2448413>
- [14] Beecken, B. P., "Development and Application of NUMIT for Realistic Modeling of Deep-Dielectric Spacecraft Charging in the Space Environment," Air Force Research Lab. AFRL-RV-PS-TR-2014-0181, April 2014.
- [15] Jun, I., Garrett, H. B., Kim, W., and Minow, J. I., "Review of an Internal Charging Code, NUMIT," *IEEE Transactions on Plasma Science*, Vol. 36, No. 5, 2008, pp. 2467–2472.
<https://doi.org/10.1109/TPS.2008.2003440>
- [16] Kim, W., Chinn, J. Z., Katz, I., Garrett, H. B., and Wong, K. F., "3-D NUMIT: A General 3-D Internal Charging Code," *IEEE Transactions on Plasma Science*, Vol. 45, No. 8, 2017, pp. 2298–2302.
- [17] Frederickson, A., "Charge Deposition, Photoconduction, and Replacement Current in Irradiated Multilayer Structures," *IEEE Transactions on Nuclear Science*, Vol. 22, No. 6, 1975, pp. 2556–2561.
<https://doi.org/10.1109/TNS.1975.4328167>
- [18] Frederickson, A., "Radiation Induced Electrical Current and Voltage in Dielectric Structures," Air Force Cambridge Research Labs. AD-A007 670, Cambridge, MA, Nov. 1974.
- [19] Beecken, B., Gibson, Z., and Cooke, D., "Toward Validation of the AF-NUMIT3 Dielectric Charging Simulation Model," *16th Spacecraft Charging Technology Conference*, April 2022.
- [20] Beecken, B. P., Greenlee, T. R., and Hoglund, R. M., "Creation and Development of a Next Generation NUMIT-Type Model that Handles Changing Conductivities and Varying Electrode Configurations," *Proc. of the 13th International Spacecraft Charging Technology Conference*, Paper 223, 2014.
- [21] Hodges, J. L., Dennison, J. R., Dekany, J., Wilson, G., Evans, A., and Sim, A. M., "In Situ Surface Voltage Measurements of Dielectrics Under Electron Beam Irradiation," *IEEE Transactions on Plasma Science*, Vol. 42, No. 1, 2013, pp. 255–265.
<https://doi.org/10.1109/TPS.2013.2291862>
- [22] Tabata, T., and Ito, R., "An Algorithm for the Energy Deposition by Fast Electrons," *Nuclear Science and Engineering*, Vol. 53, No. 2, 1974, pp. 226–239.
- [23] Wood, B., King, D., and Dennison, J. R., "Time-Evolved Constant Voltage Conductivity Measurements of Common Spaceborne Polymeric Materials," *15th Spacecraft Charging Technology Conference*, Kobe Univ., Kobe, Japan, 2018.
- [24] Gillespie, J. C., "Temperature Dependence of Radiation Induced Conductivity," Ph.D. Dissertation, Utah State Univ., Logan, UT, 2022.
- [25] Lee, J., Allen, H., and Dennison, J. R., "Real and Imaginary Permittivity Testing in High-Vacuum and Variable Temperature Settings," *Applied Space Environments Conference 2021*, Jet Propulsion Lab., Pasadena, CA, 2021.
- [26] Boman, J., Wood, B., Lee, J., and Dennison, J. R., "New System for Temperature Dependent Radiation Induced Conductivity Measurements," *Applied Space Environments Conference 2021*, 2021.
- [27] Griseri, V., Perrin, C., Fukunaga, K., Maeno, T., Payan, D., Levylevy, L., and Laurent, C., "Space-Charge Detection and Behavior Analysis in Electron Irradiated Polymers," *IEEE Transactions on Plasma Science*, Vol. 34, No. 5, 2006, pp. 2185–2190.
<https://doi.org/10.1109/TPS.2006.877209>
- [28] Hands, A. D., Ryden, K. A., Pacaud, R., Paulmier, T., Sarrailh, P., Payan, D., and Rogers, D., "Validation of Internal Charging Tools with Experiments in REEF," *IEEE Transactions on Plasma Science*, Vol. 47, No. 8, 2019, pp. 3824–3833.
<https://doi.org/10.1109/TPS.2019.2900891>
- [29] Song, S., Chen, H., Yu, X., Chen, A., Shi, W., Zou, H., and Ye, Y., "Variation of Permittivity and Dark Conductivity of Polyimide and FR4 with Electron Dose by Experiments," *IEEE Transactions on Nuclear Science*, Vol. 68, No. 9, 2021, pp. 2375–2382.
<https://doi.org/10.1109/TNS.2021.3101320>
- [30] Kim, W., Jun, I., and Kokorowski, M., "Internal Electrostatic Discharge Monitor (IESDM)," *IEEE Transactions on Nuclear Science*, Vol. 57, No. 6, 2010, pp. 3143–3147.
- [31] Wilson, G., and Dennison, J. R., "Approximation of Range in Materials as a Function of Incident Electron Energy," *IEEE Transactions on Plasma Science*, Vol. 40, No. 2, 2012, pp. 291–297.
<https://doi.org/10.1109/TPS.2011.2176515>
- [32] Gibaru, Q., Inguibert, C., Belhaj, M., Raine, M., and Lambert, D., "Monte-Carlo Simulation and Analytical Expressions for the Extrapolated Range and Transmission Rate of Low Energy Electrons [10 eV–10 keV] in 11 Monoatomic Materials," *Applied Surface Science*, Vol. 570, Dec. 2021, Paper 151154.
<https://doi.org/10.1016/j.apsusc.2021.151154>
- [33] Hastings, D., and Garrett, H. B., *Spacecraft-Environment Interactions*, Cambridge Univ. Press, Cambridge, England, U.K., 2004, Chap. 2.

- [34] Froominckx, T. B., and Sojka, J. J., "Solar Cycle Dependence of Spacecraft Charging in Low Earth Orbit," *Journal of Geophysical Research: Space Physics*, Vol. 97, No. A3, 1992, pp. 2985–2996. <https://doi.org/10.1029/91JA02704>
- [35] "APTIV 1000 Series Films for Electrical Insulation," AVPF Technology, <https://www.victrex.com/en/datasheets> [accessed 22 Dec. 2022].
- [36] Ginzel, E., and Ginzel, R., "Approximate dV/dT Values for Some Materials," *e-Journal of Nondestructive Testing (eJNDT)*, ISSN 1435-4934, 2017.
- [37] Rae, P., and Brown, E., "Some Observations on Measuring Sound Speeds in Polymers Using Time-of-Flight," *Experimental Techniques*, Vol. 40, No. 3, 2016, pp. 1085–1097. <https://doi.org/10.1007/s40799-016-0109-6>
- [38] Gibson, Z., and Dennison, J. R., "Uncertainties of the Pulsed Electroacoustic Method: Peak Positions of Embedded Charge Distributions," *2022 IEEE 4th International Conference on Dielectrics (ICD)*, July 2022, pp. 539–543. <https://doi.org/10.1109/ICD53806.2022.9863513>
- [39] Plis, E. A., Engelhart, D. P., Cooper, R., Ferguson, D. C., and Hoffmann, R., "Effect of Environment on Charge Transport Properties of Polyimide Films Damaged by High-Energy Electron Radiation," *Journal of Vacuum Science & Technology B, Nanotechnology and Microelectronics: Materials, Processing, Measurement, and Phenomena*, Vol. 36, No. 5, 2018, Paper 052906.
- [40] Mackova, A., Malinsky, P., Miksova, R., Hnatowicz, V., Khaibullin, R., Slepicka, P., and Svoricik, V., "Characterisation of PEEK, PET and PI Implanted with 80 keV Fe+ Ions to High Fluencies," *Nuclear Instruments and Methods in Physics Research Section B: Beam Interactions with Materials and Atoms*, Vol. 331, July 2014, pp. 176–181. <https://doi.org/10.1016/j.nimb.2013.12.045>
- [41] Cooper, R., and Hoffman, R., "Jumbo Space Environment Simulation and Spacecraft Charging Chamber Characterization," AFRL-RV-PS-TP-2015-0012, Air Force Research Lab., Space Vehicles Directorate, Kirtland AFB, April 2015.
- [42] Maeno, T., Futami, T., Kushibe, H., Takada, T., and Cooke, C., "Measurement of Spatial Charge Distribution in Thick Dielectrics Using the Pulsed Electroacoustic Method," *IEEE Transactions on Electrical Insulation*, Vol. 23, No. 3, 1988, pp. 433–439. <https://doi.org/10.1109/14.2384>
- [43] Hamidouche, L., Geron, E., and Hole, S., "Very High Spatial Resolution Space Charge Measurement Using Electro-Acoustic Reflectometry (EAR)," *IEEE Electrical Insulation Magazine*, Vol. 33, No. 5, 2017, pp. 9–16. <https://doi.org/10.1109/MEI.2017.8014386>
- [44] Imburgia, A., Miceli, R., Sansaverino, E. R., Romano, P., and Viola, F., "Review of Space Charge Measurement Systems: Acoustic, Thermal and Optical Methods," *IEEE Transactions on Dielectrics and Electrical Insulation*, Vol. 23, No. 5, 2016, pp. 3126–3142. <https://doi.org/10.1109/TDEI.2016.7736878>
- [45] Arnaout, M., Berquez, L., Baudoin, F., and Payan, D., "Contribution to Improving the Spatial Resolution of a Pulsed Electro Acoustic Cell Measurement: An Analysis of Acoustics Waves Propagation," *2010 10th IEEE International Conference on Solid Dielectrics (ICSD)*, Inst. of Electrical and Electronics Engineers, New York, 2010, pp. 1–4.
- [46] Griseri, V., Fukunaga, K., Maeno, T., Laurent, C., Levy, L., and Payan, D., "Pulsed Electro-Acoustic Technique Applied to In-Situ Measurement of Charge Distribution in Electron-Irradiated Polymers," *IEEE Transactions on Dielectrics and Electrical Insulation*, Vol. 11, No. 5, 2004, pp. 891–898. <https://doi.org/10.1109/TDEI.2004.1349795>
- [47] International Electrotechnical Committee, "Calibration of Space Charge Measuring Equipment Based on the Pulsed Electro-Acoustic (PEA) Measurement Principle," International Electrotechnical Committee, IEC TS 62758:2012, 2012.
- [48] Galloy, L., Berquez, L., Baudoin, F., and Payan, D., "High-Resolution Pulsed Electro-Acoustic (HR PEA) Measurement of Space Charge in Outer Space Dielectric Materials," *IEEE Transactions on Dielectrics and Electrical Insulation*, Vol. 23, No. 5, 2016, pp. 3151–3155. <https://doi.org/10.1109/TDEI.2016.7736880>
- [49] Gibson, Z., Dennison, J. R., Pearson, L., Griffiths, E., Pearson, A., and Griseri, V., "Effects of Sample Adhesives Acoustic Properties on Spatial Resolution of Pulsed Electroacoustic Measurements," *2018 IEEE Conference on Electrical Insulation and Dielectric Phenomena (CEIDP)*, Inst. of Electrical and Electronics Engineers, New York, 2018, pp. 267–270.
- [50] Chen, G., Chong, Y., and Fu, M., "Calibration of the Pulsed Electroacoustic Technique in the Presence of Trapped Charge," *Measurement Science and Technology*, Vol. 17, No. 7, 2006, p. 1974.
- [51] Pearson, L. H., Dennison, J. R., Griffiths, E. W., and Pearson, A. C., "PEA System Modeling and Signal Processing for Measurement of Volume Charge Distributions in Thin Dielectric Films," *IEEE Transactions on Plasma Science*, Vol. 45, No. 8, 2017, pp. 1955–1964. <https://doi.org/10.1109/TPS.2016.2632627>
- [52] Vazquez, A., Chen, G., Davies, A., and Bosch, R., "Space Charge Measurement Using Pulsed Electroacoustic Technique and Signal Recovery," *Journal of the European Ceramic Society*, Vol. 19, Nos. 6–7, 1999, pp. 1219–1222.
- [53] Gupta, A., and Reddy, C. C., "Critical Issues in Space Charge Estimation Using PEA System," *2016 International Conference on Condition Monitoring and Diagnosis (CMD)*, Inst. of Electrical and Electronics Engineers, New York, 2016, pp. 94–97.
- [54] Arnaout, M., Chahine, K., Paulmier, T., and Payan, D., "Model-Based Processing for the Estimation of Space-Charge Distribution from Non-Contact Pulsed Electro-Acoustic Measurements," *Journal of Electrostatics*, Vol. 114, Nov. 2021, Paper 103636. <https://doi.org/10.1016/j.elstat.2021.103636>
- [55] Posey, N. A., and Minow, J. I., "Development of a Real Time Internal Charging Tool for Geosynchronous Orbit," NASA Tech. Rept. M13-2891, Aug. 2013.
- [56] Willis, E. M., Howard, J. W., Jr., Miller, J. S., Minow, J. I., Neergard-Parker, L., and Suggs, R. M., "Recent Applications of Space Weather Research to NASA Space Missions," *2013 Space Weather Workshop*, No. M13-2586, April 2013.
- [57] Barton, D. A., Beecken, B. P., and Hoglund, R. M., "Determination of Energy and Charge Deposition Profiles in Elemental Slabs from an Isotropically Equivalent Electron Source Using Monte Carlo Simulations," *IEEE Transactions on Plasma Science*, Vol. 43, No. 9, 2015, pp. 2861–2868. <https://doi.org/10.1109/TPS.2015.2461543>
- [58] Davis, V., and Mandell, M., Nascap-2k Version 4.2 Scientific Documentation, Leidos, Inc., San Diego, CA, 2014.
- [59] Beecken, B., and Wallin, B., "Modeling of Deep-Dielectric Spacecraft Charging in Realistic Environments with NUMIT2," *3rd AIAA Atmospheric Space Environments Conference*, AIAA Paper 2011-3975, June 2011.
- [60] Chiparã, M. D., and Chiparã, M. I., "Effects of Gamma Irradiation on PTFE," *Polymer Degradation and Stability*, Vol. 37, No. 1, 1992, pp. 67–71. [https://doi.org/10.1016/0141-3910\(92\)90093-K](https://doi.org/10.1016/0141-3910(92)90093-K)
- [61] Shulman, H., and Ginell, W., "Nuclear and Space Radiation Effects on Materials," NASA SP-8053, Vol. 15, June 1970.
- [62] Perrin, C., Griseri, V., and Laurent, C., "Measurement of Internal Charge Distribution in Dielectrics Using the Pulsed Electro-Acoustic Method in Non Contact Mode," *IEEE Transactions on Dielectrics and Electrical Insulation*, Vol. 15, No. 4, 2008, pp. 958–964. <https://doi.org/10.1109/TDEI.2008.4591216>
- [63] Gibson, Z., and Dennison, J. R., "The Relevance of Pulsed Electroacoustic Measurements for Spacecraft Charging," *Spacecraft Charging Technolgy Conference*, April 2022.

T. K. Minton
Associate Editor